Hindawi
International Journal of Chemical Engineering
Volume 2023, Article ID 8667432, 11 pages
https://doi.org/10.1155/2023/8667432

Research Article

Kinetic Study of Zirconia-Alumina-Supported Ni-Fe Catalyst for Dry Reforming of Methane: Impact of Partial Pressure and Reaction Temperature

Ahmed Al-Fatesh,[1] Kenit Acharya,[2] Ahmed I. Osman,[3] Ghzzai Almutairi,[4] Anis Hamza Fakeeha,[1] Ahmed Elhag Abasaeed,[1] Yousef A. Al-Baqmaa,[1] and Rawesh Kumar[2]

[1]*Chemical Engineering Department, College of Engineering, King Saud University, P.O. Box 800, Riyadh 11421, Saudi Arabia*
[2]*Department of Chemistry, Indus University, Ahmedabad 382115, Gujarat, India*
[3]*School of Chemistry and Chemical Engineering, Queen's University Belfast, Belfast BT9 5AG, Belfast, UK*
[4]*Hydrogen Technologies Institute, King Abdulaziz City for Science and Technology (KACST), P.O. Box 6086, Riyadh 11442, Saudi Arabia*

Correspondence should be addressed to Ahmed Al-Fatesh; aalfatesh@ksu.edu.sa, Ahmed I. Osman; aosmanahmed01@qub.ac.uk, Ghzzai Almutairi; gmotari@kacst.edu.sa, and Rawesh Kumar; kr.rawesh@gmail.com

Received 26 January 2023; Revised 21 February 2023; Accepted 21 April 2023; Published 11 May 2023

Academic Editor: Pedro Castano

A better understanding of the reaction mechanism and kinetics of dry reforming of methane (DRM) remains challenging, necessitating additional research to develop robust catalytic systems with high catalytic performance, low cost, and high stability. Herein, we prepared a zirconia-alumina-supported Ni-Fe catalyst and used it for DRM. Different partial pressures and temperatures are used to test the dry reforming of methane reaction as a detailed kinetic study. The optimal reaction conditions for DRM catalysis are 800°C reaction temperature, 43.42 kPa CO_2 partial pressure, and 57.9 kPa CH_4 partial pressure. At these optimal reaction conditions, the catalyst shows a 0.436 kPa^2 equilibrium constant, a 0.7725 $mol_{CH_4}/g_{Cat}/h$ rate of CH_4 consumption, a 0.00651 $mol_{CH_4}/m^2/h$ arial rate of CH_4 consumption, a 1.6515 $mol_{H_2}/g_{Cat}/h$ rate of H_2 formation, a 1.4386 $mol_{CO}/g_{Cat}/h$ rate of CO formation. This study's findings will inspire the cost-effective production of robust catalytic systems and a better understanding of the DRM reaction's kinetics.

1. Introduction

Dry reforming of methane (DRM) has received worldwide interest in terms of its ability to reduce the concentration of greenhouse gases (CH_4 and CO_2) and its efficiency in producing an important synthetic feedstock known as "syngas" ($CO + H_2$) (reaction 1). Dry reforming of methane is a highly endothermic reaction, and it is feasible between 600 and 800°C reaction temperature [1]. The reverse water gas shift reaction (RWGS) is the most significant competitive reaction (reaction 2) with DRM. As RWGS consumes H_2, the presence of this reaction may affect the H_2 yield of the reaction. It is the responsibility of the DRM research community to optimize the reaction parameters, such as the partial pressure of each feed gas component and reaction temperature, to maximize the catalytic activity of the DRM reaction while minimizing the other parallel side reactions (such as RWGS).

$$\begin{aligned} CH_4 + CO_2 &\rightleftharpoons 2H_2 + 2CO \quad \Delta H^\circ = \frac{247.34\,\text{KJ}}{\text{mol}} \\ H_2 + CO_2 &\longrightarrow CO + H_2O \quad \Delta H^\circ = \frac{41.145\,\text{KJ}}{\text{mol}}. \end{aligned} \tag{1}$$

The DRM reaction proceeds in two steps: the dissociation of CH_4 over catalytically active sites followed by the oxidation of dissociated CH_x species by CO_2. Slow

dissociation of CH_4 results in low activity, whereas delayed oxidation leads to coke deposition over catalytic active sites, ultimately affecting the catalytic activity of the catalyst used. This necessitates that DRM scientists address both aspects, namely how to increase the catalytic active site and provide instant oxidation of carbon deposits. Metal centres such as Ni, Co, Rh, Pd, and Pt are catalytically active sites for CH_4 dissociation, with Ni having numerous advantages over the others. Ni offers low-cost preparation and has 25 times more CH_4 interaction energy than Co and less CH_4 dissociation energy than Pd and Pt [2, 3]. However, Ni sintering at high temperatures remains problematic, leading to the size growth of metallic Ni to the point of inactivation. For CH_4 decomposition over silica-supported Fe, the catalyst was inactive, whereas redox metal oxides such as ZrO_2-supported Fe catalysts were active [4, 5]. The redox property of ZrO_2 enables the support to release instant lattice oxygen during the surface reaction, thus leaving a vacancy behind. Furthermore, ZrO_2 is supposed to enhance CO_2 dissociation, forming oxygen [6, 7]. ZrO_2 may be channel oxygen flow for a surface oxidation reaction under DRM conditions of high reaction temperatures. Overall, it can be stated that Fe dispersed over ZrO_2 is responsible for CH_4 dissociation, and "CO_2 along with ZrO_2" channelizes the oxygen flow for instant oxidation of carbon deposits during the DRM reaction. ZrO_2-supported Fe catalysts achieved ~20% CH_4 conversion up to 4 h TOS [4, 5].

Interestingly, alumina-silicate (Al/Si = 80 : 20) supported Fe catalyst and alumina-supported Ni catalyst showed <5% CH_4 conversion after 4 h, >40% CH_4 conversion after 5 h, and >80% CH_4 conversion up to 5 h, respectively [4]. With increasing alumina content, acidity has increased, and high and stable CH_4 conversion has been observed. Apart from this, Fe dispersion over basic support MgO was also found to be moderately active for CH_4 decomposition [4, 8] (~60% CH_4 conversion, ~50% H_2 yield).

Fe dispersion over Al_2O_3 was highly active for CH_4 decomposition, but this catalyst system is inactive in DRM. In the presence of CO_2, the dissociation of CH_4 may be inhibited by an iron-based catalyst, as Fe is oxidized into FeO [9], which is incapable of dissociating CH_4. At the same time, in the presence of CO_2, the Ni-supported catalyst was found to be quite active for CH_4 decomposition. However, it is rapidly rendered inactive due to coke deposition. Optimizing Ni and Fe content was beneficial regarding catalytic activity and stability. Ni-Fe alloy is stable at extremely high temperatures; therefore, catalytically active metallic Ni is maintained under DRM conditions [10]. Al_2O_3-supported NiFe (3 : 1) catalyst had a specific alloy composition (Ni_3Fe), resulting in improved catalytic activity (13% CH_4 conversion after 3 h TOS) than Al_2O_3-supported Ni catalyst (8% CH_4 conversion after 3 h) at 600°C [11]. In low-temperature DRM, evaporation-induced self-assembly (EISA)-prepared NiFe catalysts supported on alumina have garnered interest. It showed 26.6% CH_4 conversion, 37.8% CO_2 conversion, and 0.67 H_2/CO ratio at 550°C [12]. Li et al. prepared a mesoporous alumina-supported NiFe (Ni/Fe = 10/7) catalyst using the EISA method and found that the catalyst was deactivated after 24 hours due to the dealloying of $FeNi_3$ [13]. Gunduz-Meric et al. prepared a coke and sinter-resistant "Ni-iron core (ratio 4 : 1) and silica sphere" catalyst [14]. Silica shell formed SiC and protects carbon decomposition in the presence of catalytically active Ni, as well as limiting Ni dispersion. It showed more than 70% CH_4 conversion and a 0.70 H_2/CO ratio for up to three cycles. Fe-modified $MgAl_2O_4$-supported Ni catalysts and $MgAl_2O_4$ supported NiFe catalysts were also tested for DRM [10, 15]. At Ni/Fe = 1.4, loaded over $MgAl_2O_4$ support, the role of iron was found to be crucial in the decoking at the metal centre [10]. Here, some of the metallic Fe is oxidized to FeO_x by CO_2. Besides, the lattice oxygen of FeO_x is superior for decoking, producing CO and metallic Fe, where the latter restores the original Fe-Ni alloy [16]. The second pathway for coke oxidation involves the dissociation of CO_2 over metallic Ni into CO and O, followed by subsequent coke oxidation by surface oxygen [9]. Ni-Al (3 : 1) supported on Mg(Al)O demonstrated >1.5 mol_{CH4} mol_{metal}^{-1} s^{-1} CH_4 conversion for up to 30 h time on stream. The effective decoking at the metal centres was due to the reaction of FeO with surface carbon [17]. Mayenite ($Ca_{12}Al_{14}O_{33}$) support Ni catalyst is prone to deactivation in DRM, but adding 2 wt.% Fe [18] effectively suppressed coke. The support may facilitate the transfer of oxygen species from FeO_x to Ni sites, thereby promoting carbon deposit oxidation.

We expect that by incorporating ZrO_2 into Al_2O_3, lattice oxygen endowing capacity will be enhanced and that by introducing Fe with Ni, effective decoking will occur. Herein, we prepare a zirconia-alumina-supported Ni-Fe catalyst. Different partial pressures and temperatures are used to test the dry reforming of methane in a detailed kinetic study. To the authors' best knowledge, this is the first detailed study to optimize the partial pressure of each feed gas component over a 700–800°C reaction temperature to maximize the DRM catalytic activity and minimize side reactions like RWGS.

2. Experimental

2.1. Catalyst Preparation. The catalyst 5Ni2Fe/ZrAl is synthesized by impregnating the required amounts of $Ni(NO_3)_2.6H_2O$ (99%; Alfa Aesar) aqueous solution (equivalent to 5 wt% NiO) and $Fe(NO_3)_3.9H_2O$ (403.99 g/mol; 99.99%; Alfa Aesar) (equivalent to 2 wt% of Fe_2O_3) with commercially available 10 wt% zirconium oxide–90 wt% alumina support. The solution was heated under stirring until a slurry was formed. It was further dried at 120°C and calcined at 700°C with a heating rate of 3°C/min for 5 hrs. The catalyst is abbreviated as 5Ni2Fe/ZrAl.

2.2. Catalyst Reaction. DRM reaction is carried out in a stainless tubular reactor (diameter 0.91 cm and length 30 cm) made by PID Eng. & Tech. Micro. Activity company. 100 mg catalyst is packed in the reactor and reduced under reductive pretreatment with H_2 (flow rate 20 ml/min) at 600°C for 1 h. The gas feed is composed of CH_4, CO_2 and N_2, which are allowed to pass through the catalyst bed at different flow rates (total flow rate = 70 ml/min) at three

different reaction temperatures (700, 750, and 800°C). The products are analyzed by a gas chromatograph equipped with a TCD detector.

The expressions for mole fraction, partial pressure, and specific feed rate of each gas are shown in supporting information S1. In this manuscript, we have studied different activity terms (shown below) at a different partial pressure of gas feed at 700°C, 750°C, and 800°C reaction temperatures. CH_4 conversion conversion, CO_2 conversion, and H_2/CO ratio are expressed by equations (4)–(6). The specific feed rate of a gas is defined as the flow rate of a gas per gram weight of catalyst. The rate of CH_4 consumption and rate of CO_2 consumption are shown by equations (6) and (7) , respectively. The details of expressions for rate of H_2 formation, rate of CO formation, and rate of H_2O formation are derived in supporting information S2 and the final expressions are shown in equations (9)–(11). The arial rate of gas consumption is defined as the rate of gas consumption per unit surface area per gram weight of catalyst. The expression for the arial rate of CH_4 consumption and the arial rate of CO_2 consumption are shown in equations (10) and (11), respectively.

$$CH_4 \text{ conversion} = \frac{CH_{4,in} - CH_{4,out}}{CH_{4,in}} \times 100\%, \tag{2}$$

$$CO_2 \text{ conversion} = \frac{CO_{2,in} - CO_{2,out}}{CO_{2,in}} \times 100\%, \tag{3}$$

$$\frac{H_2}{CO} = \frac{\text{Moles of } H_2 \text{ produced}}{\text{Moles of CO produced}}, \tag{4}$$

$$\text{Rate of } CH_4 \text{ consumption} = -R_{CH_4} = \frac{CH_4 \text{ conversion x } CH_4 \text{specific feed rate}}{100}, \tag{5}$$

$$\text{Rate of } CO_2 \text{ consumption} = -R_{CO_2} = \frac{CO_2 \text{ conversion x } CO_2 \text{ specific feed rate}}{100}, \tag{6}$$

$$\text{Rate of } H_2 \text{ formation} = R_{H_2} = R_{CO_2} - 3R_{CH_4}, \tag{7}$$

$$\text{Rate of } CO \text{ formation} = R_{CO} = -\left(R_{CH_4} + R_{CO_2}\right), \tag{8}$$

$$\text{Rate of } H_2O \text{ formation} = R_{H_2O} = R_{CH_4} - R_{CO_2}, \tag{9}$$

$$\text{Arial rate of } CH_4 \text{ consumption} = -RA_{CH_4} = \frac{R_{CH_4}}{\text{Surface area of catalyst}}, \tag{10}$$

$$\text{Arial rate of } CO_2 \text{ consumption} = -RA_{CO_2} = \frac{R_{CO_2}}{\text{Surface area of catalyst}}. \tag{11}$$

3. Results and Discussion

3.1. Characterization Results. The catalyst had a 118.6 m^2/g BET surface area and type IV adsorption/desorption isotherms with an H1 hysteresis loop (Figure 1(a)). The sharp inflection between 0.6 and 0.75 relative pressure regions in the isotherm indicates capillary condensation, an indication of uniformity of pore distribution in the mesoporous material [19, 20]. Pore size distribution over the catalyst surface is shown by the $dV/d \log W$ vs. W plot (where V is volume and W is the pore width) in Figure 1(a) (inset). The majority of the pores on the surface of the catalyst are 27 nm in size. Based on the BJH pore size measurement, the average pore size is determined to be 15.5 nm. The fresh 5Ni2Fe/ZrAl catalyst has a thermally stable tetragonal ZrO_2 phase (at $2\theta = 30$, 50, 60°; JCPDS reference number: 00-024-1164), rhombohedral Al_2O_3 phase (at $2\theta = 36.8$, 45.5, 60, 66°; JCPDS reference number: 01-077-2135), and cubic $NiAl_2O_4$ phases (at $2\theta = 30$, 36.8, 45.5, 50, 60, 66°; JCPDS reference number: 01-071-0965) (Figure 1(b)). Previously, metallic Ni derived from thermally stable $NiAl_2O_4$ (during reduction) was claimed prominent active site for high catalytic activity in DRM [21–23]. The IR spectra reveals the presence of physically adsorbed CO_2 at approximately 2349 cm^{-1} [24], carbonate species at 1384 cm^{-1}, and formate at 2850 and 2925 cm^{-1} [7] (Figures 1(c) and 1(d)). The IR peak at 1631 cm^{-1} and 3444 cm^{-1} indicates the bending and stretching vibrations of O-H, respectively [25]. Figures 1(e) and 1(f) show an HR-TEM image of a fresh and spent catalyst. The spent catalyst has carbon nanotubes with a variable diameter.

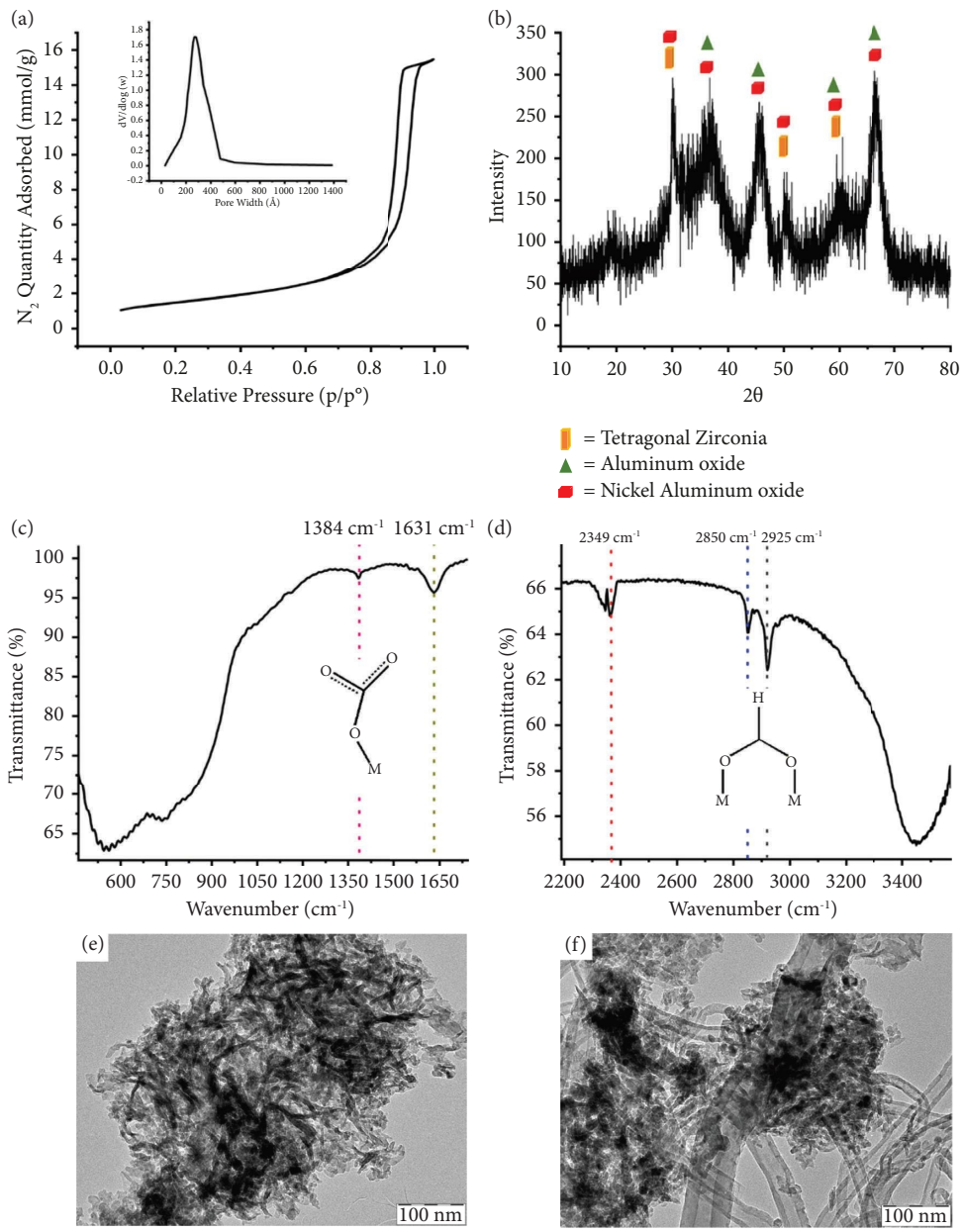

Figure 1: Characterization results of the 5Ni2Fe/ZrAl, (a) N_2 adsorption isotherm and porosity distribution profiles, (b) XRD diffractogram, (c and d) IR spectra of the catalyst, (e) HR-TEM image of fresh catalyst, and (f) HR-TEM image of spent catalyst (treated under 30 CH_4: 30 CO_2: 10 N_2 at 700°C reaction temperature).

3.2. Catalytic Activity Result and Discussion. The catalyst 5Ni2Fe/ZrAl has uniform mesopores with an average size of 15.5 nm. It possessed thermally stable support (as tetragonal ZrO_2 phase and rhombohedral Al_2O_3 phase), metallic Ni (derived from thermally stable $NiAl_2O_4$ upon reduction), catalytic active sites, and various types of "CO_2 interacting species (physically adsorbed CO_2, carbonate or formate)" over the catalyst surface [23, 24, 26]. The role of Fe-Ni was previously claimed in coke suppression [18]. A uniform mesoporous, thermally stable, metallic Ni dispersed (derived from $NiAl_2O_4$ after reduction), and CO_2-interacting catalyst surface seems efficient for the DRM and RWGS reaction. Table 1 shows the catalytic activity results of the 5Ni2Fe/ZrAl catalyst in terms of an equilibrium constant, CH_4 conversion, CO_2 conversion, and H_2/CO ratio. At low CH_4 partial pressure and high CO_2 partial pressure, CH_4 conversion is very high (Table 1, Entry 5-6, 14-15, and 23-24) due to the instant oxidation of the substrate (CH_4) by a large number of oxidants (CO_2). Similarly, at low CO_2 partial pressure and high CH_4 partial pressure, CO_2 conversion is very high (Table 1, Entry 1-2, 10-11, 19-20) due to the instant utilization of the oxidating agent (CO_2) by a large number of substrates (CH_4). From a catalytic standpoint, the "mole of CH_4 or CO_2 consumption per gram mass of catalyst per hour," "mole of CH_4 or CO_2 consumption per gram mass of catalyst per hour per surface area," and "mole of product

Table 1: The catalytic activity results at a different partial pressure of feed gas during 700, 750, and 800°C reaction temperatures.

Entries	Temp. (°C)	P_{CH_4}	P_{CO_2}	P_{N_2}	K ($\times10^{-3}$)	C_{CH_4}%	C_{CO_2}%	H_2/CO	$-R_{CH_4}$ ($\times10^{-3}$)	$-RA_{CH_4}$ ($\times10^{-3}$)	$-R_{CO_2}$ ($\times10^{-3}$)	$-RA_{CO_2}$ ($\times10^{-3}$)	R_{H_2} ($\times10^{-3}$)	R_{CO} ($\times10^{-3}$)	R_{H_2O} ($\times10^{-3}$)
1	700	43.43	14.48	43.43	9.5	39.21	82.24	1.4	288.5	2.43	201.7	1.7	663.8	490.2	—
2		43.43	21.71	36.19	4.7	36.12	70.83	0.94	265.8	2.24	260.6	2.2	536.7	526.3	—
3		43.43	28.95	28.95	3.5	36.75	62.18	0.82	270.4	2.28	305.0	2.6	506.2	575.4	34.6
4		43.43	57.9	0	2.6	43.44	46.57	0.86	319.6	2.69	456.8	3.9	502.0	776.5	137.2
5		14.48	43.43	43.43	2.6	80.06	34.54	0.72	196.3	1.65	254.1	2.1	334.9	450.5	57.8
6		21.71	43.43	36.19	4.2	69.75	44.84	0.93	256.6	2.16	329.9	2.8	439.9	586.5	73.3
7		28.95	43.43	28.95	3.6	55.78	48.43	0.79	273.6	2.31	356.3	3.0	464.5	629.9	82.7
8		57.9	43.43	0	6.9	43.08	60.28	0.94	422.6	3.56	443.5	3.7	824.3	866.1	20.9
9		50.66	50.66	0	4.8	43.34	52.51	0.82	380.6	3.21	450.7	3.8	691.1	831.3	70.1
10	750	43.43	14.48	43.43	17.7	46.325	95.1	1.86	340.8	2.87	233.2	2.0	789.3	574.1	—
11		43.43	21.71	36.19	15.1	49.95	89.62	1.41	367.5	3.10	329.7	2.8	772.8	697.2	—
12		43.43	28.95	28.95	13.3	52.765	87.44	1.2	388.2	3.27	428.9	3.6	735.8	817.1	40.7
13		43.43	57.9	0	10.9	65.785	53.41	0.8	484.0	4.08	523.9	4.4	928.1	1008.0	39.9
14		14.48	43.43	43.43	6.2	98.31	35.95	0.85	241.1	2.03	264.5	2.2	458.8	505.6	23.4
15		21.71	43.43	36.19	14.7	96.63	55.18	1.13	355.5	3.00	406.0	3.4	660.4	761.5	50.5
16		28.95	43.43	28.95	20.8	89.81	69.31	1.3	440.5	3.71	509.9	4.3	811.6	950.5	69.4
17		57.9	43.43	0	22.3	61.29	87.58	1.23	601.3	5.07	644.4	5.4	1159.4	1245.6	43.1
18		50.66	50.66	0	18.7	67.03	74.55	1.07	575.4	4.85	639.9	5.4	1086.2	1215.3	64.5
19	800	43.43	14.48	43.43	7.9	35.65	95.66	1.2	262.3	2.21	234.6	2.0	552.3	496.9	—
20		43.43	21.71	36.19	11.3	45.2	93.13	1.24	332.6	2.80	342.6	2.9	655.1	675.2	10.0
21		43.43	28.95	28.95	16.2	55.78	91.55	0.99	410.4	3.46	449.0	3.8	782.1	859.4	38.7
22		43.43	57.9	0	3.4	55.775	91.55	0.99	410.4	3.46	898.1	7.6	333.0	1308.5	487.7
23		14.48	43.43	43.43	6.2	98.5	43.815	0.62	241.6	2.04	322.4	2.7	402.3	563.9	80.8
24		21.71	43.43	36.19	15.7	98.19	60.08	0.86	361.2	3.04	442.0	3.7	641.6	803.2	80.8
25		28.95	43.43	28.95	25.9	95.295	74.615	1.1	467.4	3.94	549.0	4.6	853.3	1016.4	81.6
26		57.9	43.43	0	43.6	78.75	90.53	1.16	772.5	6.51	666.1	5.6	1651.5	1438.6	—
27		50.66	50.66	0	23.7	71.59	89.01	1.12	614.5	5.18	764.0	6.4	1079.5	1378.5	149.5

Abbreviation and unit: (1) P: pressure; kPa (2) K: equilibrium constant of DRM; $(kPa)^2$ (3) C: conversion (4) $-R$: rate of consumption; mol/g_{cat}/h (5) $-RA$: arial rate; mol/m^2/h (6) R: rate of formation; mol/g_{cat}/h.

formation per gram mass of catalyst per hour" are exact presentations of catalytic activity. Thus, furthermore, Table 1 contains catalytic activity data regarding the rate of CH_4 consumption, areal rate of CH_4 consumption, the rate of CO_2 consumption, the areal rate of CO_2 consumption, the rate of H_2 formation, the rate of CO formation, and the rate of H_2O formation at a different partial pressures of feed gas during 700, 750, and 800°C reaction temperatures.

In the dry reforming of methane, CH_4 is the substrate and CO_2 is the oxidant. Upon increasing the partial pressure of CH_4 (substrate) or CO_2 (oxidant), the rate of CH_4 and CO_2 consumption increases at reaction temperatures of 700, 750, and 800°C (Figures 2(a)–2(d)). This suggests that the presence of an increasing amount of substrate (CH_4) over a fixed oxidant (CO_2) or the presence of an increasing amount of oxidant (CO_2) over a fixed substrate (CH_4) gives rise to more collision, and a higher rate of conversion at a given temperature. At 43.43 kPa partial pressure of CH_4 and 14.48 kPa partial pressure of CO_2, the H_2/CO ratio is found to be 1.4, 1.86, and 1.2 at 700, 750, and 800°C, respectively (Table 1 Entry 1, 10, and 19). The high H_2/CO ratio at these partial pressures is due to the availability of a high concentration of CH_4 (which is primarily responsible for H_2 generation) as well as a low concentration of CO_2 (which is mainly responsible for CO generation) over the catalyst surface.

At constant CO_2 partial pressure (43.425 kPa) and increasing CH_4 partial pressure (from 14.475 to 57.9 kPa) at 800°C, the rate of CH_4 consumption is significantly increasing (Table 1 Entry 23–26, Figure 2 A). At constant 43.425 kPa CH_4 partial pressure at 800°C, the rate of CH_4 consumption increases sharply (0.2623 $mol_{CH_4}/g_{cat}/h$ to 0.4104 $mol_{CH_4}/g_{cat}/h$) up to 29 kPa CO_2 partial pressure, after which it remains constant (Table 1 Entry 19–22, Figure 2(c)). This finding needs to be explained in more detail. Upon doubling the partial pressure of CO_2 (from 28.95 kPa to 57.9 kPa), the rate of CH_4 consumption remains constant at 800°C reaction temperature, whereas the rate of CO_2 consumption doubles (0.4490 $mol_{CO_2}/g_{cat}/h$ at 28.97 kPa CO_2 partial pressure to 0.8981 $mol_{CO_2}/g_{cat}/h$ at 58 kPa CO_2 partial pressure) (Figure 2(d)). It indicates that as CO_2 partial pressure increases from 29 kPa to 58 kPa, CO_2 remains converted but does not oxidize CH_4 (as in conventional DRM reaction). In this partial pressure range, it may oxidize the H_2 or carbon deposit on the catalyst surface. Under the same conditions, the rate of hydrogen formation decreases by more than 50% (0.7821 $mol_{H_2}/g_{cat}/h$ at 28.97 kPa CO_2 partial pressure to 0.3330 $mol_{H_2}/g_{cat}/h$ at 58 kPa CO_2 partial pressure) (Figure 3(c)), the rate of CO formation increases by up to 1.5 times (0.8594 $mol_{CO}/g_{cat}/h$ at 28.97 kPa CO_2 partial pressure to 1.3085 $mol_{CO}/g_{cat}/h$ at 58 kPa CO_2 partial pressure) (Figure 3(d)) and rate of H_2O formation increases by up to 12 times (0.0387 $mol_{H_2O}/g_{cat}/h$ at 28.97 kPa CO_2 partial

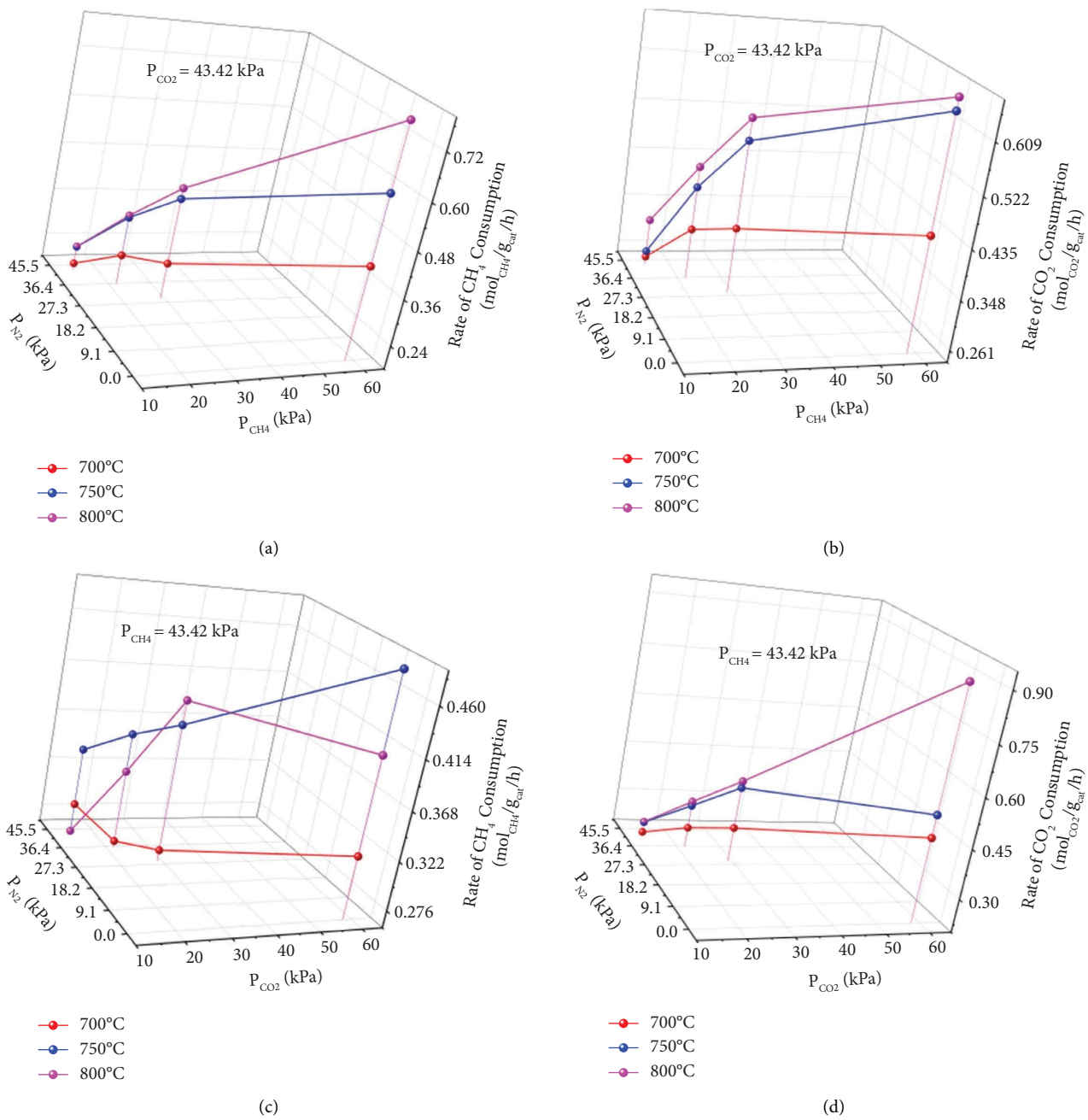

Figure 2: Catalytic activity in terms of (a) CH_4 consumption rate at constant CO_2 partial pressure (43.42 kPa), (b) CO_2 consumption rate at constant CO_2 partial pressure (43.42 kPa), (c) CH_4 consumption rate at constant CH_4 partial pressure (43.42 kPa), and (d) CO_2 consumption rate at constant CH_4 partial pressure (43.42 kPa).

pressure to 0.4877 $mol_{H_2O}/g_{cat}/h$ at 58 kPa CO_2 partial pressure) (Figure 3(f)). This observation suggests that the reverse water gas shift reaction is accelerating in the 29 kPa to 58 kPa CO_2 partial pressure range at 800°C reaction temperature, whereas the dry reforming of methane is just continuing at the same rate.

At 750°C reaction temperature and constant CH_4 partial pressure (43.42 kPa), with a rise of CO_2 partial pressure from 14.475 kPa to 28.95 kPa, the rate of CH_4 formation constantly increases (from 0.3408 $mol_{CH_4}/g_{cat}/h$ to 0.3772 $mol_{CH_4}/g_{cat}/h$), but the rate of H_2 formation decreases from 0.7893 $mol_{H_2}/g_{cat}/h$ to 0.7358 $mol_{H_2}/g_{cat}/h$, and the rate of water formation becomes significant. This observation indicates the presence of a reverse water gas shift reaction (Table 1 Entry 10–12, Figures 2(c), 3(c), and 3(f)). However, on the further increase of CO_2 partial pressure up to 57.9 kPa; a rise of rate CH_4 consumption (0.3882 $mol_{CH_4}/g_{cat}/h$ to 0.4840 $mol_{CH_4}/g_{cat}/h$), a rise in the rate of CO_2 consumption (0.4289 $mol_{CO_2}/g_{cat}/h$ to 0.5239 $mol_{CO_2}/g_{cat}/h$), a rise in the rate of H_2 formation (0.7358 $mol_{H_2}/g_{cat}/h$ to 0.9281 $mol_{H_2}/g_{cat}/h$), and a rise in the rate of CO formation (0.8171 $mol_{CO}/g_{cat}/h$ to 1.0081 $mol_{CO}/g_{cat}/h$) were achieved

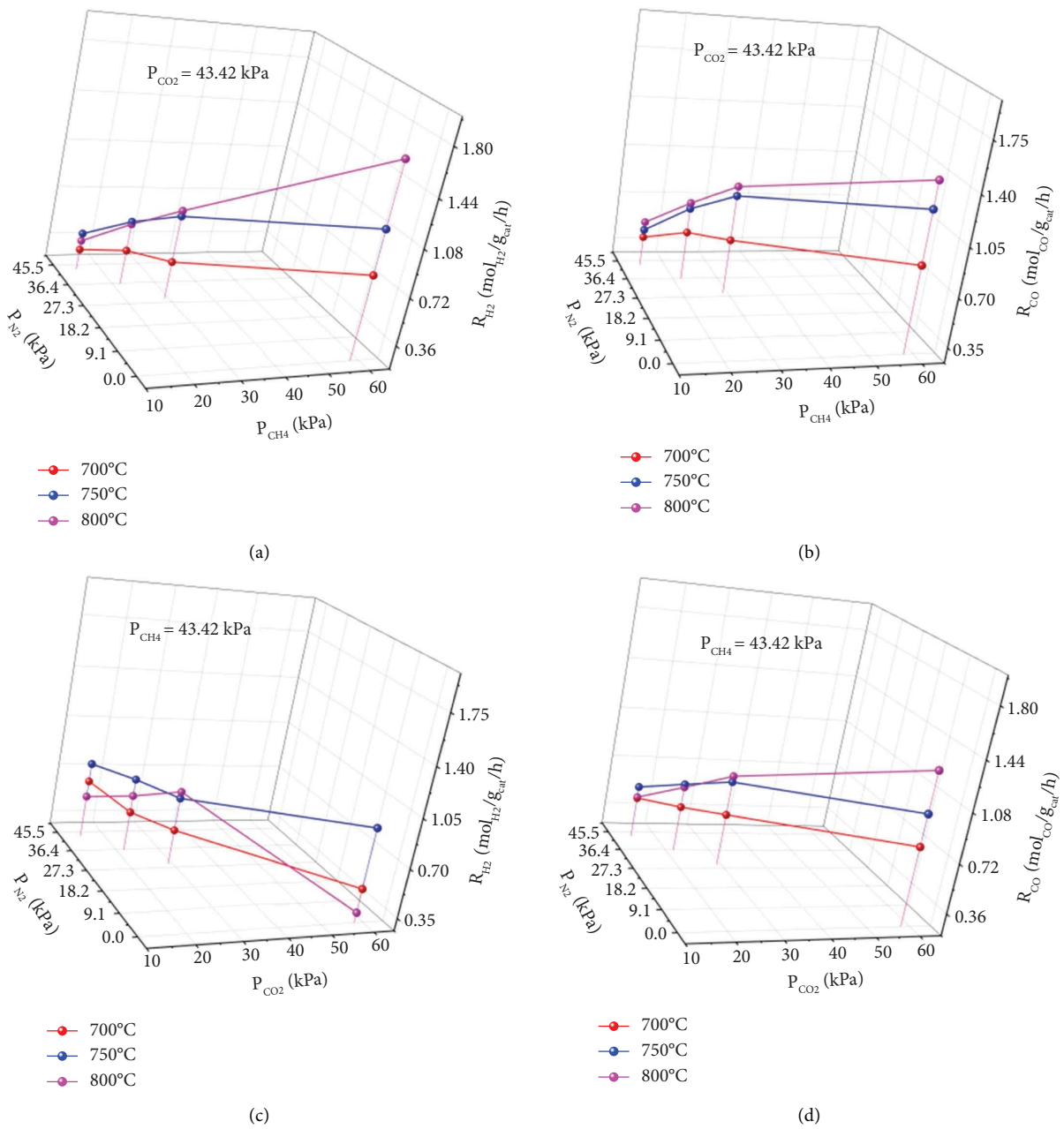

Figure 3: Continued.

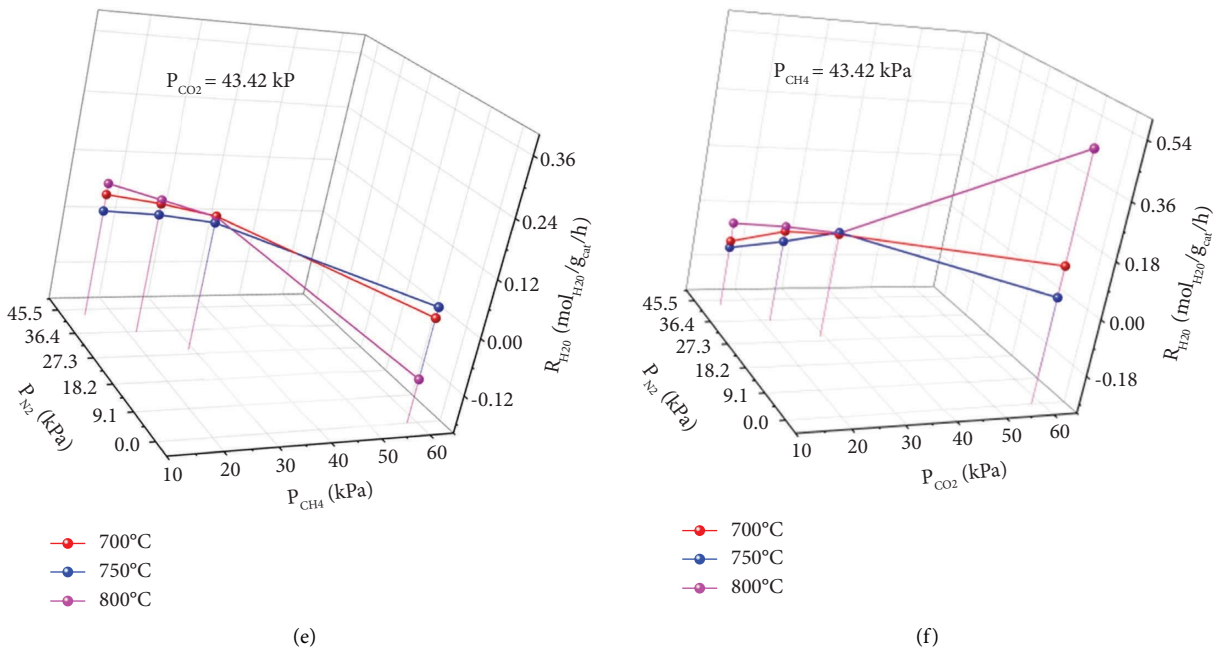

Figure 3: Catalytic activity in terms of (a) rate of H_2 formation at constant CO_2 partial pressure (43.42 kPa), (b) rate of CO formation at constant CO_2 partial pressure (43.42 kPa), (c) rate of H_2 formation at constant CH_4 partial pressure (43.42 kPa), (d) rate of CO formation at constant CH_4 partial pressure (43.42 kPa),(e) rate of H_2O formation at constant CO_2 partial pressure (43.42 kPa), and (f) rate of H_2O formation at constant CH_4 partial pressure (43.42 kPa).

without affecting the rate of H_2O formation much (Table 1 Entry 12-13, Figures 2(c), 3(c), and 3(f)). Thus, RWGS is competent up to 28.95 kPa CO_2 partial pressure, but at 57.9 kPa CO_2 partial pressure, RWGS product formation rates are not significantly affected, whereas DRM product formation rates are significantly affected. At constant CO_2 partial pressure (43.425 kPa) and increasing CH_4 partial pressure (from 14.475 kPa to 57.9 kPa) at 750°C, the rate of CH_4 consumption is increased to about ~2.5 times (0.2411 $mol_{CH_4}/g_{cat}/h$ to 0.6013 $mol_{CH_4}/g_{cat}/h$), rate of CO_2 consumption is increased to about ~2.5 times (0.2645 $mol_{CO_2}/g_{cat}/h$ to 0.6444 $mol_{CO_2}/g_{cat}/h$), the rate of H_2 formation is again increased to 2.5 times (0.4588 $mol_{H_2}/g_{cat}/h$ to 1.1594 $mol_{H_2}/g_{cat}/h$), and the rate of CO formation is again increased to about ~2.5 times (0.5056 $mol_{CO}/g_{cat}/h$ to 1.2456 $mol_{CO}/g_{cat}/h$) (Table 1 Entry 14–17, Figures 2(a), 2(b), 3(a), and 3(b)). No such progressive correlation with the rate of H_2O formation is found (Figure 3(e)), but it remains significant. It demonstrates that at 750°C reaction temperature, with constant CO_2 partial pressure and increasing CH_4 partial pressure, the dry reforming of methane reaction progressed continuously.

At a low reaction temperature of 700°C, the least activity is noticed. On constant CH_4 partial pressure (43.42 kPa) and increased partial pressure of CO_2 from 14.47 kPa to 57.9 kPa, the rate of H_2 production decreases continuously (0.6638 $mol_{H_2}/g_{cat}/h$ to 0.5020 $mol_{H_2}/g_{cat}/h$), the rate of CO formation increases continuously (0.4902 $mol_{CO}/g_{cat}/h$ to 0.7765 $mol_{CO}/g_{cat}/h$), and the rate of H_2O formation is found to a maximum of 0.1372 $mol_{H_2O}/g_{cat}/h$ at 57.9 kPa CO_2 partial pressure (Table 1 Entry 1–4; Figures 3(c)–3(f)). It indicates that at a constant CH_4 partial pressure and a rising partial pressure of CO_2 at 700°C, the RWGS product formation rate influences the DRM product formation rate. However, at constant CO_2 partial pressure (43.42 kPa) and rise of CH_4 partial pressure (14.47 kPa to 57.9 kPa), the rate of H_2 formation and rate of CO formation are increased, but no such correlation is found with the rate of water formation (Table 1 Entry 5–8; Figures 3(a), 3(b), and 3(e)). It indicates that a higher rate of H_2 and CO formation may be caused by a pronounced DRM reaction in which a portion of H_2 participates in the RWGS reaction, but this does not affect the high rate of H_2 production.

Comparing the catalytic activity results at all temperatures reveals that at 14.47 kPa CO_2 partial pressure, 43.42 kPa CH_4 partial pressure, and 43.42 kPa N_2 partial pressure, the RWGS reaction does not occur at 700°C, 750°C, and 800°C reaction temperatures. In these instances, DRM activity is, however, low. At 800°C reaction temperature, the 43.42 kPa CO_2 partial pressure and 57.9 kPa CH_4 partial pressure (with diluent N_2), the equilibrium constant of DRM is maximum (0.436 kPa^2). In this reaction condition, the RWGS reaction is not exiting, and the rate of CH_4 consumption (0.7725 $mol_{CH_4}/g_{Cat}/h$), the arial rate of CH_4 consumption (0.00651 $mol_{CH_4}/m^2/h$), the rate of H_2 formation (1.6515 $mol_{H_2}/g_{Cat}/h$), and the CO formation (1.4386 $mol_{CO}/g_{Cat}/h$) are the maximum among all tested conditions. In the mean of the maximum rate of CO_2 consumption, 57.9 kPa CO_2 partial pressure, 43.42 kPa CH_4 partial pressure and 800°C reaction temperature are found appropriate. The equal partial pressure of CH_4 and CO_2 (50.66 kPa) at 750°C, 0.6145 $mol_{CH_4}/g_{Cat}/h$ rate of CH_4 conversion, 1.0795 $mol_{H_2}/g_{Cat}/h$ rate of H_2 formation, and 1.3785 $mol_{CO}/g_{Cat}/h$ CO formation were noticed.

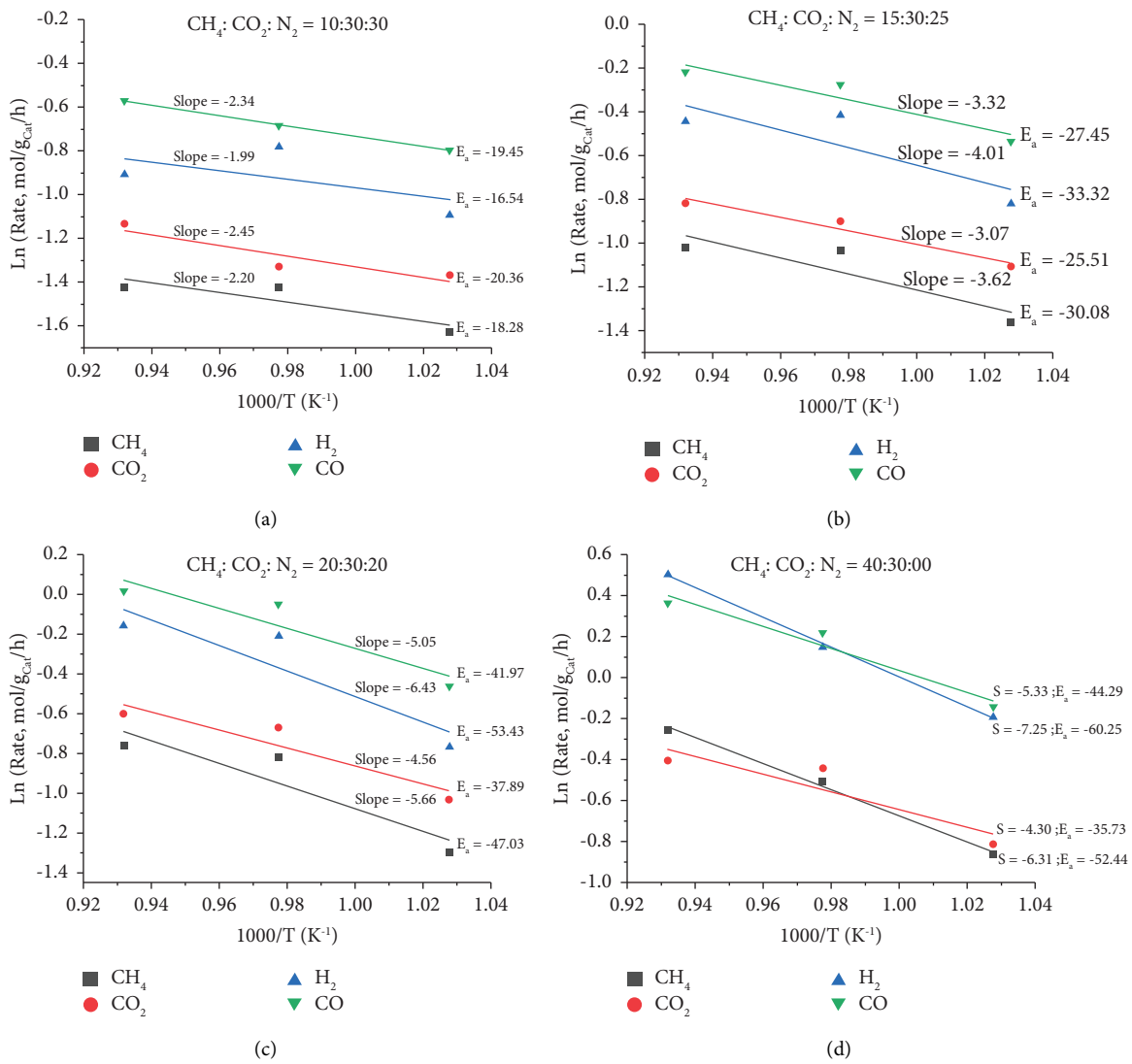

Figure 4: Influence of the reaction temperature on the CH_4 consumption rate, CO_2 consumption rate, H_2 formation rate, and CO formation rate upon fixing CO_2 flow rate (a) $CH_4:CO_2:N_2 = 10:30:30$ (b) $CH_4:CO_2:N_2 = 15:30:25$ (c) $CH_4:CO_2:N_2 = 20:30:20$ (d) $CH_4:CO_2:N_2 = 40:30:00$.

The apparent activation energy for CH_4 dissociation, CO_2 dissociation, H_2 formation, and CO formation is shown in Figure 4. It is interesting to note down that with an increasing flow rate of CH_4 from 10 ml/min to 40 ml/min and a fixed CO_2 flow rate of 30 ml/min, the apparent activation energies for CH_4 dissociation, CO_2 dissociation, and H_2 formation are increasing (Figure 4). Upon increasing the flow rate of CO_2 and fixing CH_4 flow rate at 30 ml/min, no such correlation is found (Figure S3). It indicates that the C-H dissociation of CH_4 is a rate-determining step (Figure 4 and Figure S3). The Mears criterion (for external diffusion concerning CH_4 and CO_2) and Weisz-Prater criterion (for internal diffusion for CH_4 and CO_2) values for the 5Ni2Fe/ZrAl catalyst were found < 0.1 and < 1 (in the Supporting Information S4), respectively, in every case [27]. The absence of both external and internal mass transfer limitations is found in the 5Ni2Fe/ZrAl catalyst at various gas feed rates.

4. Conclusion

The thermally stable catalytic active sites $NiAl_2O_4$ as well as the CO_2-interacting mesoporous surface of the 5Ni2Fe/ZrAl catalyst were found to be effective in the DRM reaction and a competing RWGS reaction. C-H dissociation of CH_4 is the rate-determining step. Upon different flow rates of gas feed over the 5Ni2Fe/ZrAl catalyst, external and internal mass transfer limitations are absent. At 800°C reaction temperature, the constant 43.43 kPa CH_4 partial pressure, and 28.95 to 57.9 kPa CO_2 partial pressure range, the reverse water gas shift reaction is accelerated over a zirconia-alumina-supported Ni-Fe catalyst. Again, at 750°C reaction temperature, at a constant 43.43 kPa CH_4 partial pressure and 28.95 kPa CO_2 partial pressure, RWGS is noticed. At 750°C, 43.425 kPa CO_2 partial pressure and 14.475 kPa to 57.9 kPa CH_4 partial pressure, the rate of DRM reaction is increased

to about 2.5 times. At a reaction temperature of 700°C, the catalyst's performance is diminished. The optimal reaction conditions for DRM catalysis are 800°C reaction temperature, 43.42 kPa CO_2 partial pressure, and 57.9 kPa CH_4 partial pressure. At these optimal reaction conditions, the catalyst shows a 0.436 kPa^2 equilibrium constant, a 0.7725 $mol_{CH_4}/g_{Cat}/h$ rate of CH_4 consumption, a 0.00651 $mol_{CH_4}/m^2/h$ arial rate of CH_4 consumption, a 1.6515 $mol_{H_2}/g_{Cat}/h$ rate of H_2 formation, a 1.4386 $mol_{CO}/g_{Cat}/h$ rate of CO formation. On increasing the flow rate of CH_4, the apparent activation energy for CH_4 dissociation, CO_2 dissociation and H_2 formation are increasing which indicates that C-H dissociation of CH_4 is a rate-determining step in DRM over a 5Ni2Fe/ZrAl catalyst. The mass transfer limitation is absent over this catalyst.

Data Availability

No underlying data were collected or produced in this study.

Disclosure

The views and opinions expressed in this paper do not necessarily reflect those of the European Commission or the Special EU Programmes Body (SEUPB).

Conflicts of Interest

The authors declare that they have no conflicts of interest.

Acknowledgments

The authors would like to extend their sincere appreciation to Researchers Supporting Project number (RSP2023R368), King Saud University, Riyadh, Saudi Arabia. KA and RK acknowledge Indus University, Ahmedabad, India, for supporting research. Ahmed I. Osman wishes to acknowledge the support of The Bryden Centre Project (Project ID VA5048), which was awarded by The European Union's INTERREG VA Programme, managed by the Special EU Programmes Body (SEUPB), with match funding provided by the Department for the Economy in Northern Ireland and the Department of Business, Enterprise and Innovation in the Republic of Ireland. The authors would also like to thank Charlie Farrell for proofreading the manuscript.

Supplementary Materials

The expression for mole fraction, partial pressure, and specific feed rate of each gas is shown in Supporting Information S1. The detail expressions for rate of H_2 formation and rate of CO formation are shown in Supporting Information S2. Fig. S3 shows influence of the reaction temperature on the CH_4 consumption rate, CO_2 consumption rate, H_2 formation rate and CO formation rate upon fixing CH_4 flow rate. Supporting Information S4 shows calculation of mass transfer limitation. (*Supplementary Materials*)

References

[1] A. S. Al-Fatesh, Y. Arafat, S. O. Kasim, A. A. Ibrahim, A. E. Abasaeed, and A. H. Fakeeha, "In situ auto-gasification of coke deposits over a novel Ni-Ce/W-Zr catalyst by sequential generation of oxygen vacancies for remarkably stable syngas production via CO_2-reforming of methane," *Applied Catalysis B: Environmental*, vol. 280, Article ID 119445, 2021.

[2] M. S. Liao, C. T. Au, and C. F. Ng, "Methane dissociation on Ni, Pd, Pt and Cu metal (111) surfaces - a theoretical comparative study," *Chemical Physics Letters*, vol. 272, no. 5-6, pp. 445–452, 1997.

[3] G. S. Gallego, C. Batiot-Dupeyrat, J. Barrault, E. Florez, and F. Mondragón, "Dry reforming of methane over $LaNi_{1-y}B_yO3^{\pm\delta}$ (B = Mg, Co) perovskites used as catalyst precursor," *Applied Catalysis A: General*, vol. 334, no. 1-2, pp. 251–258, 2008.

[4] A. S. Al-Fatesh, A. A. Ibrahim, A. M. AlSharekh, F. S. Alqahtani, S. O. Kasim, and A. H. Fakeeha, "Iron catalyst for decomposition of methane: influence of Al/Si ratio support," *Egyptian Journal of Petroleum*, vol. 27, no. 4, pp. 1221–1225, 2018.

[5] A. S. Al -Fatesh, S. O. Kasim, A. A. Ibrahim et al., "Catalytic methane decomposition over ZrO_2 supported iron catalysts: effect of WO_3 and La_2O_3 addition on catalytic activity and stability," *Renewable Energy*, vol. 155, pp. 969–978, 2020.

[6] S. Ivanova, V. Pitchon, and C. Petit, "Application of the direct exchange method in the preparation of gold catalysts supported on different oxide materials," *Journal of Molecular Catalysis A: Chemical*, vol. 256, no. 1-2, pp. 278–283, 2006.

[7] S. Therdthianwong, C. Siangchin, and A. Therdthianwong, "Improvement of coke resistance of Ni/Al_2O_3 catalyst in CH_4/CO_2 reforming by ZrO_2 addition," *Fuel Processing Technology*, vol. 89, no. 2, pp. 160–168, 2008.

[8] A. S. Al-Fatesh, S. Barama, A. A. Ibrahim, A. Barama, W. U. Khan, and A. Fakeeha, "Study of methane decomposition on Fe/MgO-based catalyst modified by Ni, Co, and Mn additives," *Chemical Engineering Communications*, vol. 204, no. 7, pp. 739–749, 2017.

[9] S. A. Theofanidis, R. Batchu, V. V. Galvita, H. Poelman, and G. B. Marin, "Carbon gasification from Fe-Ni catalysts after methane dry reforming," *Applied Catalysis B: Environmental*, vol. 185, pp. 42–55, 2016.

[10] S. A. Theofanidis, V. V. Galvita, H. Poelman, and G. B. Marin, "Enhanced carbon-resistant dry reforming Fe-Ni catalyst: role of Fe," *ACS Catalysis*, vol. 5, pp. 3028–3039, 2015.

[11] K. Ray, S. Sengupta, and G. Deo, "Reforming and cracking of CH_4 over Al_2O_3 supported Ni, Ni-Fe and Ni-Co catalysts," *Fuel Processing Technology*, vol. 156, pp. 195–203, 2017.

[12] Z. Song, Q. Wang, C. Guo et al., "Improved effect of Fe on the stable NiFe/Al2O_3 catalyst in low-temperature dry reforming of methane," *Industrial & Engineering Chemistry Research*, vol. 59, no. 39, pp. 17250–17258, 2020.

[13] B. Li, Y. Luo, B. Li, X. Yuan, and X. Wang, "Catalytic performance of iron-promoted nickel-based ordered mesoporous alumina FeNiAl catalysts in dry reforming of methane," *Fuel Processing Technology*, vol. 193, pp. 348–360, 2019.

[14] G. Gunduz-Meric, S. Kaytakoglu, and L. Degirmenci, "Catalytic performance of silica covered bimetallic nickel-iron encapsulated core-shell microspheres for hydrogen production," *International Journal of Hydrogen Energy*, vol. 45, no. 60, pp. 34547–34556, 2020.

[15] H. Wang, N. V. Srinath, H. Poelman et al., "Hierarchical Fe-modified $MgAl_2O_4$ as a Ni-catalyst support for methane dry reforming," *Catalysis Science and Technology*, vol. 10, no. 20, pp. 6987–7001, 2020.

[16] S. M. Kim, P. M. Abdala, T. Margossian et al., "Cooperativity and dynamics increase the performance of NiFe dry reforming catalysts," *Journal of the American Chemical Society*, vol. 139, no. 5, pp. 1937–1949, 2017.

[17] T. Margossian, K. Larmier, S. M. Kim, F. Krumeich, C. Müller, and C. Copéret, "Supported bimetallic NiFe nanoparticles through colloid synthesis for improved dry reforming performance," *ACS Catalysis*, vol. 7, no. 10, pp. 6942–6948, 2017.

[18] R. Peng, Y. Chen, B. Zhang et al., "Tailoring the stability of NiFe/mayenite in methane – carbon dioxide reforming," *Fuel*, vol. 284, Article ID 118909, 2021.

[19] S. Rahman, N. Enjamuri, R. Gomes et al., "Aerobic Baeyer-Villiger oxidation of cyclic ketones over periodic mesoporous silica Cu/Fe/Ni/Co-HMS-X," *Applied Catalysis A: General*, vol. 505, pp. 515–523, 2015.

[20] S. Rahman, S. Shah, C. Santra et al., "Controllable synthesis of niobium doped mesoporous silica materials with various morphologies and its activity for oxidative catalysis," *Microporous and Mesoporous Materials*, vol. 226, pp. 169–178, 2016.

[21] L. Zhou, L. Li, N. Wei, J. Li, and J. M. Basset, "Effect of $NiAl_2O_4$ formation on Ni/Al_2O_3 stability during dry reforming of methane," *ChemCatChem*, vol. 7, no. 16, pp. 2508–2516, 2015.

[22] R. Benrabaa, A. Barama, H. Boukhlouf et al., "Physicochemical properties and syngas production via dry reforming of methane over $NiAl_2O_4$ catalyst," *International Journal of Hydrogen Energy*, vol. 42, no. 18, pp. 12989–12996, 2017.

[23] N. Ichikuni, D. Murata, S. Shimazu, and T. Uematsu, "Promoting effect of $NiAl_2O_4$ for supported Ni particles on sprayed Ni/Al_2O_3 catalysts," *Catalysis Letters*, vol. 69, no. 1/2, pp. 33–36, 2000.

[24] N. D. Parkyns, "Influence of thermal pretreatment on the infrared spectrum of carbon dioxide adsorbed on alumina," *Journal of Physical Chemistry A*, vol. 75, no. 4, pp. 526–531, 1971.

[25] L. Vlaev, D. Damyanov, and M. Mohamed, "Infrared spectroscopy study of the nature and reactivity of a hydrate coverage on the surface of γ-Al2O3," *Colloids and Surfaces*, vol. 36, no. 3, pp. 427–437, 1989.

[26] Y. Kitano, Y. Mori, A. Ishitani, and T. Masaki, "Rhombohedral phase in Y_2O_3-partially-stabilized ZrO2," *Journal of the American Ceramic Society*, vol. 71, no. 1, pp. C-34–C-36, 1988.

[27] H. S. Fogler, *Elements of Chemical Reaction Engineering*, Prentice Hall, New Jersey, USA, 4th edition, 2005.